Design and assessment of microlenslet-array relay optics

Vesselin Shaoulov and Jannick P. Rolland

Recent progress in micro-optics fabrication and optical modeling software opens the opportunity to investigate how microlenslet-array-based compact relay systems can be designed and assessed. We present various optical configurations that include an appropriate baffle computation to eliminate ghost images, followed by an analysis of image quality. The investigation shows the existing trade-off between compactness of the system and a tiling effect observed in the corresponding image, an effect we refer to as lensletization. To yield meaningful optical modeling results, we provide insight into ray-tracing optimization while ensuring a sufficient signal-to-noise ratio. The results show that, given no discernable lensletization, the most compact configuration to image gray-scale images is the 5*f*-based system. Finally, simulations of the imaging of gray scale and color bitmaps through microlenslet arrays are demonstrated for the first time to our knowledge.

OCIS codes: 350.3950, 100.2960, 110.4280.

1. Introduction

Real-time special effects in photography and moviemaking will benefit from the design of compact relay lenses.[1,2] Recent progress in micro-optics fabrication offers a potential new solution based on microlenslet arrays. The basic theory of imaging with microlenslet arrays, developed by Anderson, was driven by requirements of optical scanning devices.[3] In his research, Anderson demonstrated that arrays of simple lenses combined with appropriate baffles could be used in closeup imaging systems for black-and-white document copiers, oscilloscope cameras, as well as binary code scanners. Microlenslet-array-based imaging systems were consequently further investigated for optical scanners and copiers,[3–5] three-dimensional integral photography,[6] printers,[7] and photolithography.[8] To our knowledge the imaging capabilities of microlenslet arrays for either gray-scale or color images have not been investigated, and in this paper we provide a comprehensive investigation of 1:1 compact relays for such images.

Many optical imaging applications require extremely compact, lightweight, and cost-effective relay systems. Such applications include relaying images in head-mounted displays[9] and modifying an intermediary image plane in photographic cameras for real-time special effects,[10] two applications driving our research that do not have any stringent resolution requirements in the relaying process. With conventional design techniques, even some of the most compact relay 1:1 systems, such as those based on Fresnel and Marco lenses used in closeup imaging, present an overall length of the order of 80 mm.[11] To overcome such restrictions in overall length, an alternative approach had to be investigated. Optical relay systems based on microlenslet arrays can provide a useful solution for such applications.

In this paper we first present various first-order paraxial layouts for 1:1 imaging and associated baffle placement to eliminate ghost images. We then detail technical aspects of the simulations with respect to how rays are precisely being traced to maximize efficiency and how many rays are necessary to obtain high signal-to-noise (SNR) ratio images. We then quantify image quality in terms of lensletization, a tiling effect that can be observed in images formed with microlenslet arrays. Such a tiling effect, which highly degrades image quality, is dominant in certain first-order layouts. The first steps to image quality assessment in such systems is thus to establish conditions for minimized tiling, and in this context to discuss the compactness, the resolution limit imposed by diffraction, and the optical aberrations of such

The authors are with the School of Optics, Center for Research and Education in Optics and Lasers, University of Central Florida, 400 Central Florida Boulevard, Orlando, Florida 32816. V. Shaoulov's e-mail address is vesko@odalab.ucf.edu.

Received 4 August 2003.
0003-6935/03/346838-08$15.00/0

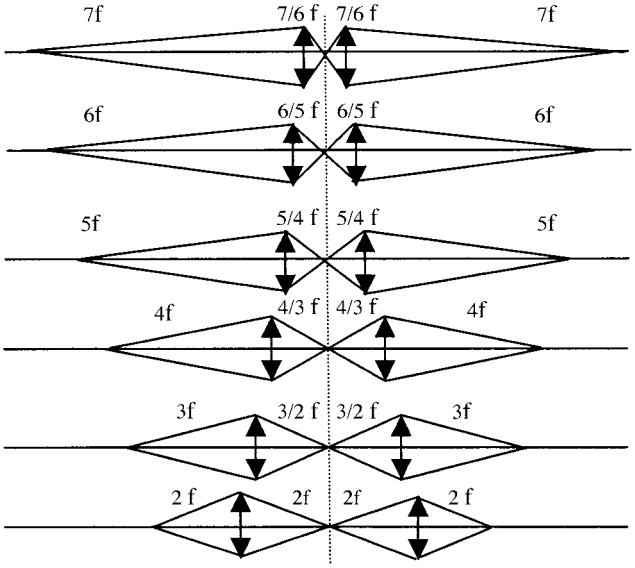

Fig. 1. Paraxial layouts of 1:1 imaging with a single pair of microlenses.

systems. This research expands on an earlier investigation reported at the International Optical Design Conference (2002) where we showed the capability of microlenses to form gray-scale images.[1] New material presented in this paper includes a comprehensive optimization of ray tracing for maximum efficiency, a SNR analysis, a quantification of lensletization, and a discussion of compactness and image quality degradations caused by diffraction and optical aberrations.

2. Paraxial Layout of 1:1 Imaging with a Pair of Microlenses

Many possible configurations of two lenses satisfy 1:1 image relay conditions. The difference among them lies in the overall length of the optical system and its field of view (FOV). The arrangements investigated in this paper are shown in Fig. 1. For all systems we consider that each pair of lenses is of the same focal length f and the same diameter D. In this case, the overall length denoted as OAL of such a system defined as the distance from the object to the final image plane is given by

$$\mathrm{OAL} = \frac{2x^2}{|x| - |f|}, \tag{1}$$

where x is the distance from the object to the first lens in each pair.

The minimum of the function given by Eq. (1) takes place at $|x|$ equal to $2|f|$, which yields the most compact configuration. Thus the most compact possible arrangement is the $2f$–$4f$–$2f$, hereafter referred to as the $2f$ system, in which the object is located at a distance $2f$ in front of the first lens and an intermediary image is formed at a distance $2f$ after the first lens with a magnification of -1, which is consequently imaged at a distance $2f$ after the second lens with a magnification of -1. Thus the total magnification of the system is $+1$. Given the symmetry of the systems, the full FOV (in millimeters), defined as 100% vignetting at its edge, is most generally given by

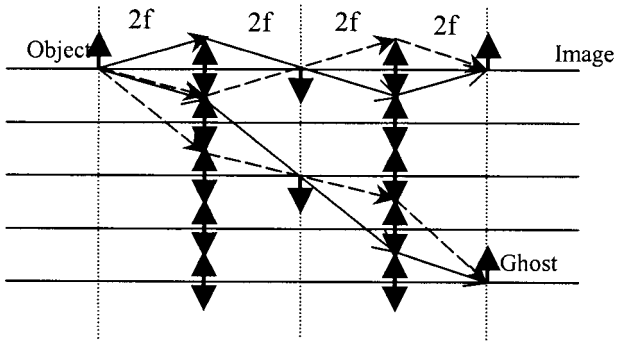

Fig. 2. Ray sketching illustrating the presence of ghost images for a stack of two microlenslet arrays without baffles.

$$\mathrm{FOV} = (M - 1)D, \tag{2}$$

where M denotes the system type, e.g., for the $2f$ system M is equal to 2 and the full FOV is equal to the diameter of the lens D.

3. Optical Layout of 1:1 Imaging with a Stack of Two Microlenslet Arrays

The concept shown in Fig. 1 is simple and compact, yet it cannot be simply extended to arrays of lenses because of the formation of ghost images.[3] The formation of ghost images is illustrated in Fig. 2 with the most compact arrangement, which is the $2f$ system, where five elements in each array are considered for illustration. The ray trace demonstrates 1:1 image formation as well as multiple ghost images. Thus appropriate baffle arrays must be used in combination with the arrays of lenses to prevent ghost images.

To determine the location and size of the appropriate baffles, we consider the $2f$ system shown in Fig. 1. We denote the first and second lens L_1 and L_2, respectively. From the theory of pupils and stops, we observe that both L_1 and L_2 limit equally the amount of light entering the system from a considered point object on axis; thus any one of them can be chosen as the aperture stop (AS), the other one being automatically the window.[12,13] Let us assume without loss of generality that L_1 is the AS of the system. The exit pupil of the optical system is by definition the image of the AS in image space. From the Descartes imaging equations, the location and size of the exit pupil for the $2f$ system are calculated to be at $4/3\,|f|$ after the second lens and three times smaller than the diameter of L_1, respectively. Similarly, the location of the entrance window is computed as the image of L_2 through L_1. Placing baffles at the locations of the entrance window or the exit pupil, whose sizes must satisfy the imaging conditions, prevents ghost-image formation. In his investigation, Anderson had proposed baffles at both locations; however, one set of

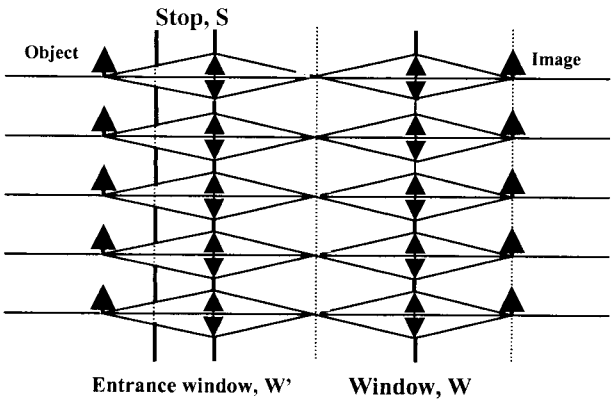

Fig. 3. Microlenslet arrays 1:1 imaging 2*f* system with the appropriate baffle to minimize ghost images.

baffles is sufficient given that they are the optical conjugate of each other.[3] This simplification, validated in the simulations presented in this paper, will bring benefits to the cost of fabrication and packaging. One of the two possible locations of the baffle for the 2*f* system (i.e., a baffle located at the entrance window) is shown in Fig. 3. With the appropriate baffle, we predict a ghost-free image formation of each object point.

A property of optical imaging with a stack of two microlenslet arrays is the sampling of the object by each pair of microlenslets in the stacks, where each pair operates over a limited FOV given by Eq. (2). Using a paraxial layout, we show the image formation with a stack of two arrays in Figs. 4(a) and 4(b) for the 2*f* and 3*f* systems, respectively. It is only through the entire stack that the entire FOV is imaged, and increasing the overall FOV requires simply the addition of more lenses to each array, while the imaging properties of the system are left otherwise invariant. Under the most compact configuration, it is shown in Fig. 4(a) that the imaged subfields of view through each pair of microlenslets do not overlap, thus creating gaps in the irradiance distribution of the final image, whereas the effect is less pronounced, if existent, for the other systems. This new effect in optical imaging with microlenslet arrays, to our knowledge first demonstrated here in images, is denoted as lensletization. To overcome this effect, an overlap of the subfields of view for each individual pair of microlenses is required at the expense of compactness and the natural loss in resolution that accompanies the overlapping subfields of view. Further analysis is presented in Subsection 4.B to quantify the effect of lensletization on image quality for the configurations. Given an extended small object seen by each lenslet, lensletization decreases with increased vignetting induced by the baffle and the amount of overlap of the subimages formed by contiguous lenslets. For example, in the 2*f* system the FOV of each individual pair of lenses measured in the object plane is equal to the aperture of the lens, and therefore pronounced lensletization occurs. As the overlap of the subfields of view increases, lensletization decreases at the expense of a loss in compactness. Such a trade-off is further investigated in Section 6. In the configurations with overlapping subfields of view (i.e., $M > 2$), the presence of varying vignetting across the subfields as well as the effect of optical aberrations on each point seen by multiple lenslets do not allow for the modeling and evaluation of the lensletization effect as a simple convolution.

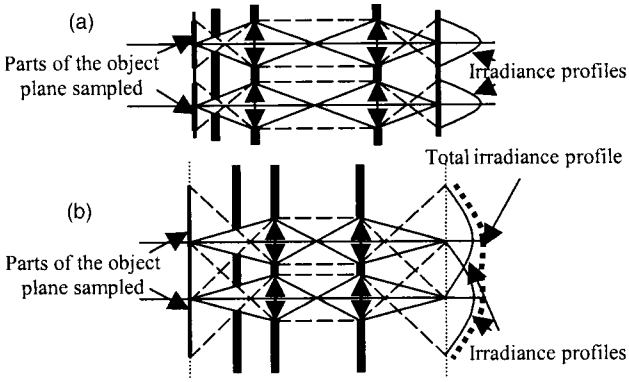

Fig. 4. Illustration of the irradiance profiles of an extended object imaged through a (a) 2*f*- and (b) 3*f*-system microlenslet array relay lens.

4. Modeling the Imaging Properties of the System with Simple Light Sources

The imaging properties of microlenslet arrays were further analyzed with a computer model for imaging that was developed with custom-designed software based on the ASAP kernel. The first aspect of modeling is to define the light source or equivalently an object to be imaged. To first gain insight into basic imaging properties such as image resolution, noise, and lensletization, we selected as an initial light source a white ellipse on a black background, which allows simple metrics to be used to quantify image quality. Consequently, more complex gray-scale light sources, such as bitmap portraits, are presented to comprehensively assess the gray-scale imaging capability of microlenslet arrays. In the case of gray-scale images, image quality can be assessed subjectively as well as with the difference between the relayed image and the initial image (i.e., also referred as the object).

The optical layout of a 2*f* system with two arrays of 11 by 11 microlenses in each array combined with an associated baffle, located without loss of generality before the lenslet arrays, is shown in Fig. 5. Furthermore, each lens in the array is a square $F/5$ plano–convex lens, 0.15 mm thick, and 5 mm in focal length. Because we use simple plano–convex singlets, which inherently have significant axial chromatic aberration, we consider imaging only one color gray-scale image, which we selected without loss of generality to be λ equal to 656 nm. Such parameters, combined with an elliptically shaped light source, are used in all the simulations presented in this section.

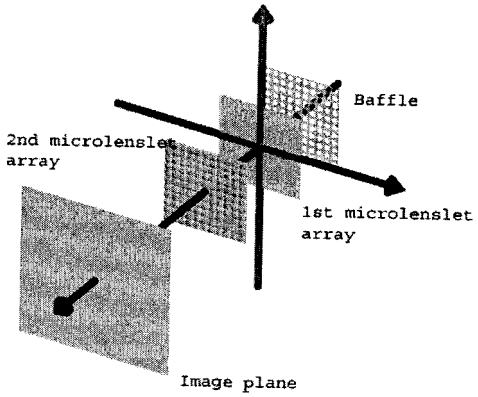

Fig. 5. ASAP layout of the 2*f*-system microlenslet-array-based relay system with two 11 by 11 arrays of microlenses and the appropriate baffle. The object to be imaged is not represented in the figure; however, shown from right to left are the baffle, the two microlenslet arrays made of plano–convex square lenses, and the detector upon which an image will be formed given the object in front of the baffle.

A. Establishing a Minimum Number of Rays

In ray-tracing-based simulations, noise can be modeled per Bernoulli's trials, a probability law that describes whether a ray reaches the detector. Let us consider the noise associated with each pixel in the detector. In this case, the probability of a ray reaching a pixel is small with respect to 1, and the probability density of noise associated with a pixel reduces to a Poisson distribution.[14] Thus the standard deviation of the noise is equal to the square root of the number of rays per pixel n in the image plane. Given the quantification of ray-tracing efficiency, the SNR in the imaging process, which varies as the square root of n, enables us to select a minimum number of rays emitted per pixel in object space.

Let us denote η as the efficiency of ray tracing defined as the ratio of the total number of rays reaching the detector plane over the total number of the rays x emitted from the object and N as the total number of pixels in the object and thus in the image. The SNR as a function of x can then be expressed as

$$\mathrm{SNR(dB)}(x) = 10 \log_{10}\left(\sqrt{\frac{x}{N}\,\eta}\right). \tag{3}$$

To further quantify the SNR as a function of the number of rays per pixel (i.e., $n = x/N$), we need to first quantify the efficiency η that varies with both the optical configuration and the specifics of the optical ray-tracing approach, hereafter referred to as the approach. For the most optimum approach, the efficiency increases from approximately 5% in the 2*f* configuration to 40% in the 7*f* configuration, respectively. However, if it can be shown to vary in the most optimum approach, it necessarily varies in the other suboptimum approaches. One suboptimum approach is when no optimization is established in a bitmap ray trace. In this case, the efficiency of the process is extremely low. For example, for the 5*f* system, 0.4% efficiency was established as detailed in the next paragraph. Thus, to limit the simulations to 1% Poisson noise, or equivalently a SNR of 100 (20 dB), approximately 2×10^{20} rays would need to be traced for a 91 by 91 pixels bitmap object. With a standard 2.0-GHz processor, such a calculation would take approximately six weeks.

We then evaluated the losses in the system and thus efficiency by setting a test detector surface consecutively at different planes and evaluating the number of rays reaching the test surface. The ray trace started with a given number of rays emitted from the object. Then the loss per element was evaluated as a function of the difference between the number of rays just before and just after each optical element. Such ray tracing allowed us to identify the surfaces where the actual loss of rays occurred and determine the overall efficiency of the ray trace. The results produced showed that, out of 100% rays on the test surface just before the first baffle, the overall efficiency of the ray trace was estimated to be 0.4% in this case.

One level of optimization in optical ray-tracing procedures is to direct the rays toward the entrance pupil of the optical system. Although in the case of microlenslet arrays no single pupil exists but instead many subpupils must be considered, a fictive pupil is defined that encompasses all the subpupils. Rays are directed toward the fictive pupil, which we accomplished by placing a diffuser in front of the object. Such a diffuser captures all rays emitted from the object before scattering and redirects them toward the entrance fictive pupil of the optical system. Such optimization increased the efficiency of the ray trace by a factor of approximately 45 (e.g., from 0.4% to 17.5% for the 5*f* system), which still required the tracing of approximately 500 million rays for a 91 by 91 pixels object. A property of this scattering technique is that each ray reaching the diffuser splits into one parent ray, which propagates according to Snell's law of refraction, and at least one child ray, which is generated uniformly within the cone defined by the fictive pupil.

Building on this scattering technique, which is standard in ASAP software, we further optimized the ray trace by splitting it in two separate ray traces. The rays were first traced from the source to the diffuser, then only the child, or scattered rays (i.e., as opposed to both the parent and the child rays), were ray traced from the diffuser toward the entrance fictive pupil of the system. This last optimization further increased the overall efficiency of the ray trace by a factor of approximately 2 (i.e., the efficiency was 34% for the 5*f* system) from the last optimization or a factor of 90 from the original unoptimized ray tracing. The SNR(x) for the most efficient ray-tracing approach is shown in Fig. 6 for the 5*f* system. Results show that 100 million rays, which is feasible to trace within a day, yield a SNR of 18 dB, or equivalently 1.6% noise. To satisfy 1% of noise in the final ray trace, ray tracing 250 million rays would still be required. In the simulations presented, we traced 100

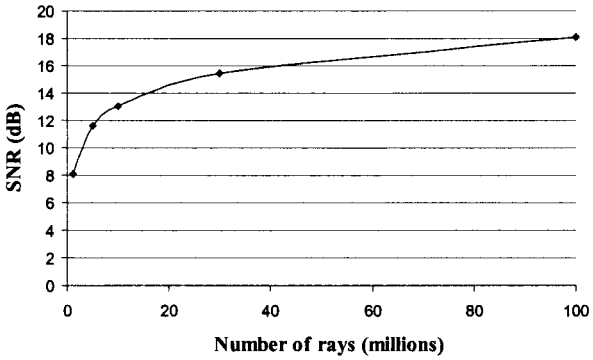

Fig. 6. SNR for the 5*f* system as a function of the number of rays emitted from the object, obtained with Eq. (3). In this plot N equal 8281 pixels and η equals 34%.

million rays, which produced results with less than 5% noise across all configurations. Such a noise level allowed for the evaluation of the image quality of the system while it kept the duration of a single ray trace within the range of a few hours.

Results of our simulations using an elliptical light source and 100 million rays are shown in Fig. 7 for the various imaging configurations reported in Fig. 1. Figure 7 also reports additional analysis of the simulations as we discuss in Subsection 4.B.

B. Quantification of Lensletization

We quantify the lensletization effect, defined in Section 3, by computing the normalized autocorrelation function of the image as well as the normalized autocorrelation function of the original object for a cross section through the center of both the object and the image (i.e., the ellipse), as shown in Figs. 7(a)–7(g). The computed normalized autocorrelation functions from the images obtained with the various configurations were subtracted from the normalized autocorrelation function of the object to assess the departure of the autocorrelation function of the image from its expected value. In Fig. 7(a) we present the object, the irradiance distribution along the central cross section, and the computed normalized autocorrelation function. In Fig. 7(b) we present the image obtained for the 2*f* system, the irradiance distribution along the central cross section, the computed normalized autocorrelation function, and the subtracted normalized autocorrelation function of the object and the image. Similar functions are shown for the other configurations in Figs. 7(c)–7(g).

The effect of lensletization due to the microlenses in the array is observed as an oscillating curve in the subtracted autocorrelation functions. The lensletization in the image of the 2*f* system, as well as the 3*f* system, although less pronounced, is clearly observed. Although the 2*f* system is most compact, the lensletization makes this configuration unsuitable to image gray-scale images. Lensletization subjectively appears to be negligible for the 4*f* system and becomes even less pronounced as expected for the 5*f*, 6*f*, and 7*f* systems. Quantitatively, we computed both the peak-to-valley (P-V) error in the subtracted normalized autocorrelation function and the rms error. The data obtained are presented in Table 1. Results show that both the P-V and rms errors are twice as large or higher for configurations below the 5*f* system. We can establish in these simulations that a P-V $<2\%$ in the subtracted autocorrelation or a rms error of $<0.6\%$ in rms leads to negligible lensletization. In the case of the simulations presented, the propagation of noise from the images to the autocorrelation function was found to be negligible, which is consistent with the results of both the P-V and rms errors presented. In this case of low noise, both the P-V and rms errors may quantify the lensletization effect. In the case of noisier images, further investigation would be required to quantify how noise in the images propagates to the autocorrelation function to establish whether the P-V would still be an acceptable measure of lensletization. The rms error intrinsically includes both the lensletization effect and the standard deviation of the noise in the computed autocorrelation.

5. Modeling of the Imaging Properties of the System for Gray-Scale Images

We created the imaging simulations with gray-scale objects (i.e., bitmap images) using the various imaging configurations presented in Fig. 1. The number of rays used was 100 million rays as well. The results are shown in Fig. 8. The modeling of the imaging of gray-scale bitmaps through the microlenslet arrays is demonstrated here for the first time to our knowledge. The challenge with imaging gray-scale bitmap images is that no artifact such as apparent lensletization is tolerable in the image. Therefore the range of optical configurations yielding no apparent artifacts must be established. In the case of binary images (i.e., black-and-white patterns), simple postprocessing operations on the images such as thresholding can be applied to recover necessary image quality for the task at hand (e.g., recognizing a letter). Such processing is not applicable to gray-scale images, and a fundamental question was whether a system can be designed to eliminate lensletization artifacts, while preserving sufficient image quality in terms of resolution, and to represent sufficiently a range of gray scales. It has been only through this investigation of imaging gray-scale images that the issue of irradiance variations in the image, which we have further defined as lensletization, has become critical to the system optimization. Results indicate that artifacts of the microlenslet arrays are observed in the 2*f*, 3*f*, and 4*f* systems, which is consistent with the results obtained and quantified for the ellipse light source. No artifacts seem observable for the 5*f*, 6*f*, and 7*f* systems.

An analysis of the image quality of the 5*f* system shows that the diffraction-limited point-spread function (PSF) is 33 μm, which in the simulation is less than the pixel size in the image (i.e., 55 μm). Given that simple plano–convex singlets were considered in the simulations, the monochromatic (i.e., λ equal to

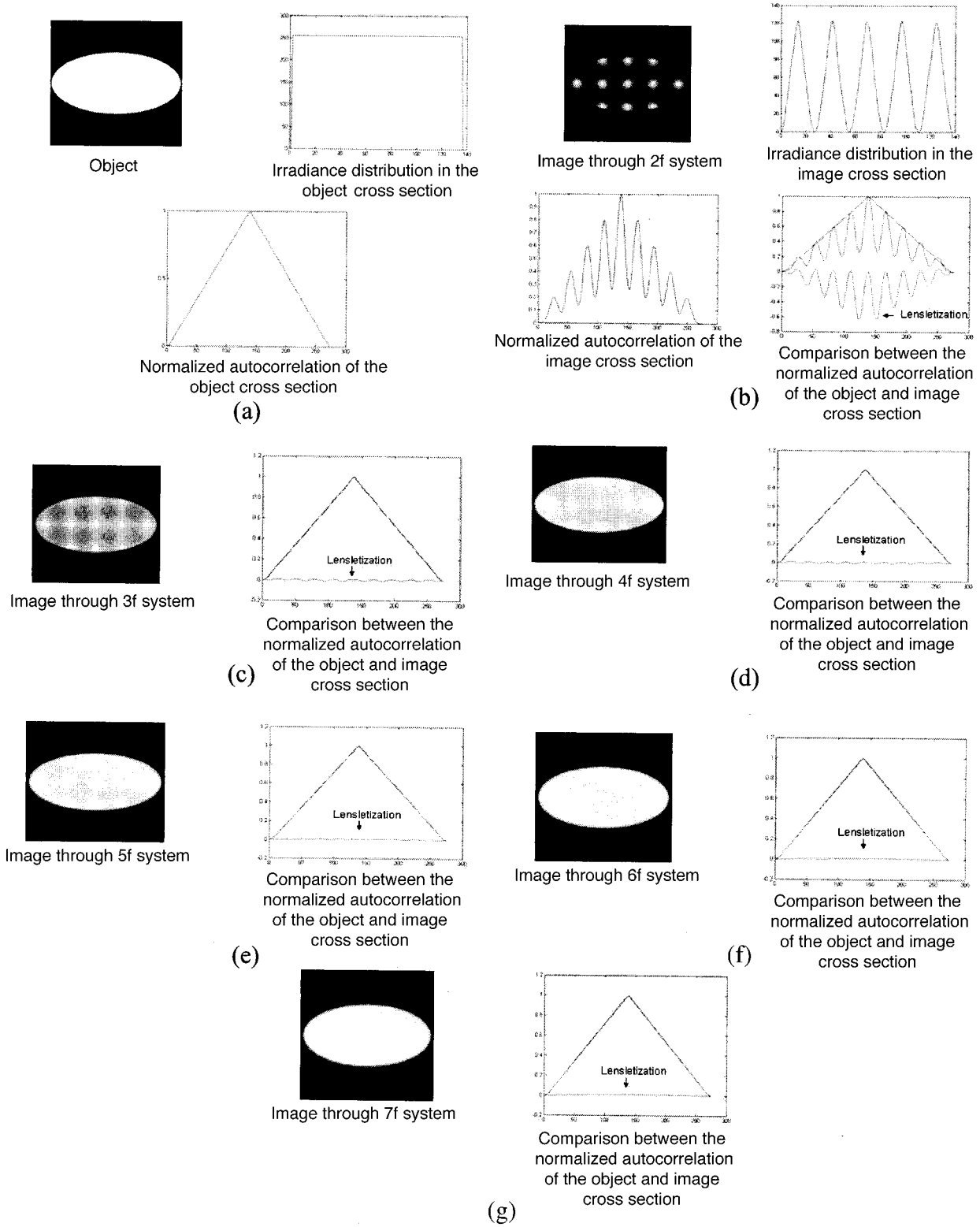

Fig. 7. Imaging and irradiance distribution of an ellipse: (a) original image; (b) image through the 2*f* system, (c) image through the 3*f* system, (d) image through the 4*f* system, (e) image through the 5*f* system, (f) image through 6*f* system, (g) image through the 7*f* system. For the irradiance distributions, the gray-level value versus the number of pixels in the object is plotted. The autocorrelation functions of the image are plotted in arbitrary units.

656 nm) modulation transfer function is found to hold reasonably well across the subfields of view of each pair of microlenses in the stack. The modulation transfer function satisfies 20% modulation at 18 cycles/mm up to 80% of the full FOV. The equivalent PSFs shown in Fig. 9 for the 0%, 70%, 95%, and 100%

Table 1. P-V Error in the Difference of the Normalized Autocorrelation of the Object and the Image

System Configuration	P-V	Error
2*f*	0.675	0.182
3*f*	0.020	0.006
4*f*	0.020	0.006
5*f*	0.009	0.002
6*f*	0.009	0.003
7*f*	0.010	0.003

vignetted FOVs illustrate the broadening of the PSF with FOV. Furthermore, the system is not fully symmetrical around the AS, and the local distortion across each subfields of view is computed to be less than 10% up to 70% of the full subfields of view and 25% at the edge of each subfield of view. Finally, given that each lenslet is a singlet and the system is not symmetric around the pupil, the system currently suffers from both axial and lateral chromatic aberrations. A simulation of a red, green, and blue (i.e., λ equal to 656, 587, and 486 nm, respectively) self-emitting image is shown in Fig. 10. Per the simulation, the overall chromatic aberrations are shown to contribute additional blur to the image in its present unoptimized stage.

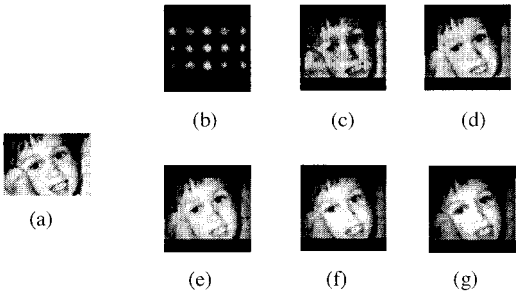

Fig. 8. Imaging and irradiance distribution of a gray-scale bitmap object: (a) original image, (b) image through the 2*f* system, (c) image through the 3*f* system, (d) image through the 4*f* system, (e) image through the 5*f* system, (f) image through the 6*f* system, (g) image through the 7*f* system.

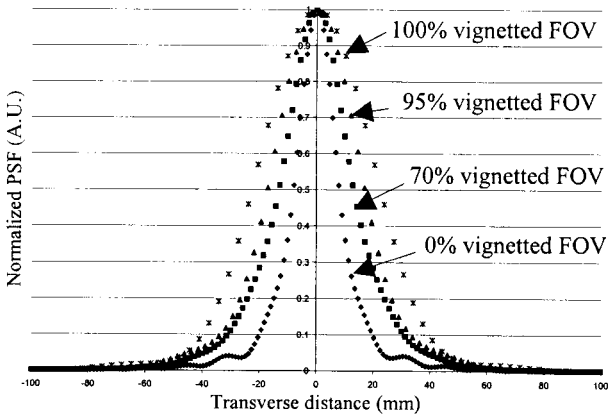

Fig. 9. Normalized PSF plots for 0%, 70%, 95%, and 100% vignetted subfields of view for a pair of plano–convex lenses.

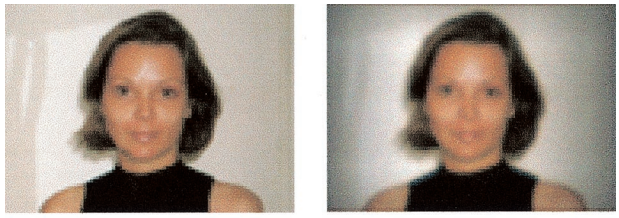

Fig. 10. Simulation of the imaging of red-green-blue image through a stack of two microlenslet arrays to qualitatively assess the impact of chromatic aberrations on image formation.

6. System Compactness

Assuming a thin-lens approximation, the compactness of each configuration, defined as the OAL from the light source to the image plane, is given by

$$\mathrm{OAL} = \frac{2M^2}{M-1}|f|, \tag{4}$$

where the OAL is shown to scale linearly with focal length. If we set the focal length of each microlens to 0.5 mm according to commercially available microlenslet arrays and we consider the 5*f* system that yields no lensletization, the OAL is only 6.25 mm. Results of compactness computations as a function of the system configuration (i.e., the M parameter) are reported in Table 2.

7. Discussion and Future Research

Although relaying images by use of such compact optical systems can be done only at the expense of resolution, such technology offers new solutions for applications in which resolution is not a stringent requirement. Such relay systems may find application in the improved design of head-mounted displays, as well as optical special effects investigated in our laboratory.[10] Specifically, in the case of relaying images in head-mounted displays, slight loss in resolution can help depixelization of the microdisplay generating the images. Thus this is a case in which a slight loss in the resolution benefits the system. In the case of optically created special effects, the images created will be highly distorted and blurred by optical phase plates inserted out of focus within the relay optics to generate images modified with special effects such as painterly effects.[1,10] In such an imaging framework, resolution is not a key qualifier of

Table 2. Overall Compactness of the Microlenslet Array Relay Configurations

Type of System	OAL (mm) for f = 0.5 mm
7*f*	8.2
6*f*	7.2
5*f*	6.25
4*f*	5.3
3*f*	4.5
2*f*	4.0

image quality, but artifacts such as lensletization must be avoided.

Future studies will further expand the research to investigate how stacks of microlenslet arrays can be optimized to satisfy various image quality criteria from the 5*f* to the 7*f* configurations, in which lensletization was shown to be negligible. Aspherization of the singlets may be used to minimize spherical and astigmatic aberrations, two main limiting monochromatic Seidel aberrations. Given that the sine condition is satisfied for these kinds of system, coma will be zero once spherical aberration is corrected. Also, whether it is possible to design better systems by stacking more than two microlenslet arrays is a question yet to be investigated. For any modification of the most basic configuration, trade-offs of image quality and cost of alignment and fabrication must be evaluated across specific application requirements. Axial color can be corrected by use of doublet lenslets within each stack. Such improvement requires a new fabrication process, which is under investigation in our laboratory.

Recent developments of ASAP software allow simulations to be run on a cluster of computers, which we may capitalize on for efficiency. Finally, this research will be extended to special effects imaging, which requires a comprehensive development of how general optical phase plates can be best modeled.[10]

8. Conclusion

In this paper we investigated the image forming capability of microlenslet arrays assembled in a relay 1:1 optics form by optical modeling and simulations. Results demonstrate the existing trade-off among noise, lensletization, image blur, and compactness. Results show that the most compact system with negligible lensletization effect is the 5*f* system. For typical 0.5-mm focal-length $F/5$ microlenses, the compactness of the 5*f* system was found to be 6.25 mm. As the FOV increases, more lenslets are added to the array, but the compactness is invariant. In its most basic and unoptimized form with respect to optical aberrations, the system image quality is shown to be limited by spherical aberration, astigmatism, and axial chromatic aberrations, which can be minimized with a stack of two aspherized doublet lenslets.

We thank BRO Corporation for the educational license of ASAP to the School of Optics at the Center for Research and Education in Optics and Lasers, as well as Mari Cote, Carey Portnoy, and Steve Miller for their assistance during the process of optimization of the ASAP code. We thank Kevin Thompson and Bill Casserly from Optical Research Associates for suggesting microlenslet arrays for relay imaging and for providing stimulating discussions about noise associated with ray tracing, respectively. We thank Ty Olmsted for his assistance in the early computer modeling part of this research. An earlier experimental study to gain insight into microlenslet imaging was supported in 2000 by the state of Florida I4 High Tech Corridor Initiative. This research was supported by the U.S. Army Simulation, Training, and Instrumentation Command.

References

1. V. Shaoulov and J. Rolland, "Compact relay lenses using microlenslet arrays," in *International Optical Design Conference 2002*, P. K. Manhart and J. M. Sasian, eds., Proc. SPIE **4832,** 74–79 (2002).
2. J. P. Rolland, H. Hua, and V. Shaoulov, "Design of a compact relay lens," Tech. Rep. TR02–05 (University of Central Florida, Orlando, Fla., 2002).
3. R. H. Anderson, "Close-up imaging of documents and displays with lens arrays," Appl. Opt. **18,** 477–484 (1979).
4. M. Kawazi and Y. Ogura, "Application of gradient index fiber arrays to copying machines," Appl. Opt. **19,** 1105–1112 (1980).
5. M. Toyama and M. Takami, "Luminous intensity of a gradient-index lens array," Appl. Opt. **21,** 1013–1016 (1982).
6. N. Davies, M. McCormick, and M. Brewin, "Design and analysis of an image transfer system using microlens arrays," Opt. Eng. **33,** 3624–3633 (1994).
7. J. Mir, "High resolution optical-addressing device and electronic scanner and/or printer apparatus employing such device," U.S. patent 4,377,753 (22 March 1983).
8. R. Volkel, H. P. Herzig, P. Nussebaum, R. Dandliker, and W. Hugle, "Microlens array imaging system for photolithography," Opt. Eng. **35,** 3323–3330 (1996).
9. H. Hua, A. Girardot, C. Gao, and J. P. Rolland, "Engineering of head-mounted projective displays," Appl. Opt. **39,** 3814–3824 (2000).
10. V. Shaoulov, C. Meyer, Y. Argotti, and J. P. Rolland, "Optical phase plates as a creative media for special effects in images," in *Novel Optical Systems Design and Optimization IV*, J. M. Sasian and P. K. Manhart, eds., Proc. SPIE **4442,** 112–118 (2001).
11. V. Belvard and P. Revy, "Optical zooming lens," U.S. patent 3,970,368 (20 July 1976).
12. P. Mouroulis and J. Macdonald, "Geometrical Optics and Optical Design," (Oxford U. Press, New York, 1997), pp. 94–108.
13. J. P. Rolland, V. Shaoulov, and F. J. Gonzalez, "The art of back-of-the-envelope paraxial raytracing," IEEE Trans. Educ. **44,** 365–372 (2001).
14. ASAP Technical Guide Radiometric Analysis, Breault Research Organization, Tucson, Ariz. (2002), pp. 43–45.